80
3-17-66

IDO-17083
February 1966

MASTER

MEASUREMENT OF THE ABSOLUTE VALUE OF ETA FOR U-233, U-235 and Pu-239 USING MONOCHROMATIC NEUTRONS

J. R. Smith, S. D. Reeder and R. G. Fluharty

RELEASED FOR ANNOUNCEMENT
IN NUCLEAR SCIENCE ABSTRACTS

PHILLIPS PETROLEUM COMPANY

PHILLIPS 66

ATOMIC ENERGY DIVISION

NATIONAL REACTOR TESTING STATION

US ATOMIC ENERGY COMMISSION

DISCLAIMER

This report was prepared as an account of work sponsored by an agency of the United States Government. Neither the United States Government nor any agency Thereof, nor any of their employees, makes any warranty, express or implied, or assumes any legal liability or responsibility for the accuracy, completeness, or usefulness of any information, apparatus, product, or process disclosed, or represents that its use would not infringe privately owned rights. Reference herein to any specific commercial product, process, or service by trade name, trademark, manufacturer, or otherwise does not necessarily constitute or imply its endorsement, recommendation, or favoring by the United States Government or any agency thereof. The views and opinions of authors expressed herein do not necessarily state or reflect those of the United States Government or any agency thereof.

DISCLAIMER

Portions of this document may be illegible in electronic image products. Images are produced from the best available original document.

PRINTED IN USA. PRICE $3.00. AVAILABLE FROM THE CLEARINGHOUSE FOR FEDERAL SCIENTIFIC AND TECHNICAL INFORMATION, NATIONAL BUREAU OF STANDARDS, U. S. DEPARTMENT OF COMMERCE, SPRINGFIELD, VIRGINIA

LEGAL NOTICE

This report was prepared as an account of Government sponsored work. Neither the United States, nor the Commission, nor any person acting on behalf of the Commission:

A. Makes any warranty or representation, express or implied, with respect to the accuracy, completeness, or usefulness of the information contained in this report, or that the use of any information, apparatus, method, or process disclosed in this report may not infringe privately owned rights; or

B. Assumes any liabilities with respect to the use of, or for damages resulting from the use of any information, apparatus, method, or process disclosed in this report.

As used in the above, "person acting on behalf of the Commission" includes any employee or contractor of the Commission, or employee of such contractor, to the extent that such employee or contractor of the Commission, or employee of such contractor prepares, disseminates, or provides access to, any information pursuant to his employment or contract with the Commission, or his employment with such contractor.

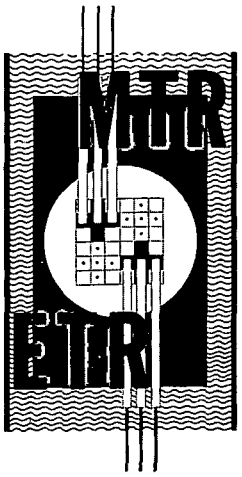

IDO-17083
AEC Research and Development Report
Physics
TID-4500 (47th Ed.)
Issued: February 1966

RELEASED FOR ANNOUNCEMENT

IN NUCLEAR SCIENCE ABSTRACTS

MEASUREMENT OF THE ABSOLUTE VALUE OF ETA FOR U-233, U-235 and Pu-239 USING MONOCHROMATIC NEUTRONS

by

J. R. Smith, S. D. Reeder and R. G. Fluharty

PHILLIPS
PETROLEUM
COMPANY

Atomic Energy Division
Contract AT(10-1)-205
Idaho Operations Office
U. S. ATOMIC ENERGY COMMISSION

THIS PAGE

WAS INTENTIONALLY

LEFT BLANK

Measurement of the Absolute Value of Eta
for U-233, U-235 and Pu-239 Using Monochromatic Neutrons

by

J. R. Smith, S. D. Reeder and R. G. Fluharty

A B S T R A C T

The absolute value of eta, the number of fission neutrons per absorption, has been measured for U-233, U-235 and Pu-239, using monochromatic neutrons from the crystal spectrometer at the Materials Testing Reactor (MTR). Measurements were made on all three isotopes at 0.025 eV neutron energy, and on U-233 and Pu-239 at 0.057 eV. The Bragg beam from Be (0002) was passed through a mechanical monochromator to remove higher order neutrons and yield a truly monochromatic beam. The neutron detector was a manganous sulphate bath, which absorbed in turn the Bragg beam and then the fission neutrons produced when the beam was completely absorbed in a fissionable sample. The ratio of the levels of Mn-56 activities produced in the two types of irradiation yielded the value of eta for the fissionable material of the sample, after the application of a few small corrections. The method of least squares was used to extract the values of eta from the experimental data. These values are at 0.025 eV: for U-233, 2.298 $\pm$ 0.009; for U-235, 2.079 $\pm$ 0.010; for Pu-239, 2.108 $\pm$ 0.008. At 0.057 eV: for U-233, 2.288 $\pm$ 0.009; for Pu-239, 2.034 $\pm$ 0.009.

CONTENTS

LIST OF FIGURES

LIST OF TABLES

Measurement of the Absolute Value of Eta for U-233, U-235 and Pu-239 Using Monochromatic Neutrons

J. R. Smith, S. D. Reeder and R. G. Fluharty

I. Introduction

Among the many parameters describing the fission characteristics of an isotope, none is more significant to reactor theory and application than η, the number of fission neutrons produced per neutron absorbed in the material. Not only does η appear in the basic four-factor formula for criticality, but it is the definitive fission parameter involved in determining the breeding ratio of a breeder system. For these reasons, many experiments have been performed to measure the absolute value of η for one or more of the three common fissionable isotopes U-233, U-235 and Pu-239[1]. The energy variation of η is of interest because of its effect on the temperature coefficient of reactivity of a reactor, and so has itself been investigated in several experiments[1]. The absolute measurements previously performed have used a reactor spectrum of neutrons. Corrections for spectral effects have been made on the basis of the results of the experiments measuring the relative energy variation.

The present experiment measured for the first time the absolute value of η using monochromatic neutrons at two different energies. The technique, which was similar to that of the Macklin-deSaussure[2] experiment, used a manganous sulphate bath as the neutron detector. A monochromatic neutron beam was totally absorbed in a fissionable sample. The fission neutrons arising from these absorptions were themselves totally absorbed in the surrounding manganese bath. The resulting Mn-56

activity was a measure of the number of fission neutrons produced. When the fissionable sample was not present, the incident beam passed into the solution, where it produced a Mn-56 activity proportional to the number of neutrons absorbed by the sample in the previous irradiation. The ratio of the two activities yielded the value of η for the sample, after the application of a few small corrections to be discussed below.

Measurements of the value of η for U-233 and Pu-239 were made at both 0.025 eV and 0.057 eV neutron energies. The value for U-235 was measured only at 0.025 eV.

II. Experimental Description

A. Monochromator

Monoenergetic neutrons were obtained from the Bragg beam of the Materials Testing Reactor (MTR) crystal spectrometer. A mechanical neutron filter[3] was used to remove neutrons of undesirable orders from the beam. Because of the presence of the filter, it was possible to utilize the high reflectivity of the Be (0002) planes. These planes are commonly neglected because of their extraordinary order problems. Not only are the undesirable orders present in large abundance, but under certain conditions the phenomenon of multiple Bragg scattering[4] ("umweganregung"), synthesizes the normally forbidden first and third order reflections. In the present case it is the second order neutrons that are desired, and the third order neutrons that represent the greatest obstacle to the isolation of the desired reflection. While a resolution $\Delta\lambda/\lambda = 1$ is adequate to isolate the first order from the second order, a resolution of 1/2 is required to isolate the second order in the presence of the third.

The neutron filter was a straight-slot velocity selector of the type described by Dash and Sommers[5]. The slots were two inches high and twenty-one inches long. A helical pitch was approximated by setting the rotor at an angle to the Bragg beam. Weight and friction were minimized by using magnesium and fiberglas in construction and mounting the motor integrally with the rotor so that only two bearings were required in the system. The construction was essentially as described previously[3], except that only 150 slots were used. This rotor matched the collimation of the neutron beam used in the experiment and had an observed transmission of 60%, while retaining adequate resolution to suppress the unwanted order neutrons at both energies used in the experiment. Rotor speed was 6000 rpm at 0.025 eV and 7200 rpm at 0.057 eV.

The purity of the beam passed by the rotor was demonstrated by time-of-flight analysis of the Bragg beam. For this test a Fermi-type chopper, placed ahead of the velocity selector, separated the neutrons into bursts whose time of flight to the detector was measured and recorded by a TMC analyzer. The resulting neutron spectra used in the experiment at the two energies are illustrated in Fig. 1. In each case there is only the primary component of the Bragg beam rising above the background level. It is clearly seen that there is no "higher order" problem with the beam transmitted through the filter.

B. Manganese Bath

1. Mechanical Features

The neutron detector was a bath of $MnSO_4$ solution contained in a cylindrical tank 42 in. in inside length and dismeter. This tank is shown in Fig. 3. At the center of the tank was the target chamber, a sphere 6 in. in diameter. This sphere was supported by an aluminum

channel, which also served to admit the neutron beam to the sample chamber, or snout, as its odd appearance led it to be called. An extension of the snout, of somewhat lighter construction, removed the impact area of the beam from the immediate vicinity of the sphere, for irradiations in which the snout contained no sample. To minimize scattering and absorption of the beam, this sample snout was flushed and filled with helium at about 7 pounds per square inch gauge pressure.

Two different sample snouts were used during various phases of this experiment. Both are shown in Fig. 4. Each has a one-inch-thick flange, by which it was bolted to the front of the tank. The view in the photograph shows the snouts as they would be seen by one looking down from the port on the top of the tank. Snout No. 1, on the right, was designed to accommodate samples of a variety of shapes and sizes. It is loaded from the top in order not to disturb the collimation system when changing samples. Because of the strain to which it is subjected during sample changeovers, its construction is relatively heavy. The entrance channel was made of 0.250 in. Al, the sphere 0.080 in., the extension .120 in., and the end cap .030 in. The sample holders used in the principal part of this experiment with the heavy snout are shown in Fig. 5. The rectangular holder accommodated a pair of Pu samples already available at the MTR, while the round holder was used with a set of samples obtained from ORNL. The latter samples were the ones fabricated for use in the Macklin-deSaussure experiment[2].

The lighter snout, shown on the left in Fig. 4, would accommodate only the ORNL samples. Since it was designed for only one set of samples, it could be made of lighter material to minimize the effects

of structural absorption. The aluminum thicknesses used in the construction of this snout are: entrance channel 0.058 in., sphere 0.030 in., extension 0.035 in., and end cap 0.010 in. This snout was loaded from the front of the tank, using the sample holder shown between the two snouts in Fig. 3. While it became necessary to remove a section of collimator between the rotor and the tank to change samples with this system, realignment errors were minimized by clamping the collimator against a set of fixed stops that remained in place during sample changeover. The reproducibility of the collimator positioning was better than 0.010 in. in any direction.

The standard configuration in which the round samples were arranged used four foils of nominal thickness 0.025 in. Two of these were contained in individual cans of aluminum 0.008 in. thick. The remaining two were mounted together, with a backing foil of 0.020 in. cadmium to absorb the residual beam. The sample thus had three sections, held at fixed distances apart by spacers to reduce the multiplication of fast neutrons. The spacers used in the sample holder for the light snout were of 0.010 in. cadmium. For the heavy snout sample holders shown in Fig. 5 aluminum spacers were used. Protection from thermal neutrons reflected from the solution was in this case afforded by a wrapping of 0.005 in. cadmium. Figure 6 shows the standard sample configuration, and Table I gives the dimensions appropriate to the various samples and spacers.

There were a few variations from the configurations indicated in the preceding paragraph. The rectangular plutonium sample had only two foils and the spacing between these was provided by the framework of the sample holder. A wrap of 0.005 in. cadmium provided protection

from the thermalized neutrons in the surrounding solution. This sample was occasionally used reversed, with the beam striking the thicker foil. This was done to change the magnitude of the fast effect and to determine whether the calculated correction would properly account for the observed change in solution activity. A corresponding experiment was performed with the U-233 sample by omitting all spacers. In addition, the two-foil U-233 sample was used alone with varying lengths of cadmium spacers behind and wrappings around it. From the latter data were determined the parameters for calculating the effects of the cadmium spacers and wrappings.

2. Chemistry of the Solution

The manganese solution was prepared from Mallinckrodt "Analytical Reagent" $MnSO_4 \cdot H_2O$ powder and demineralized water. The nominal concentration desired was 218 grams $MnSO_4$ per liter of solution. The true concentration drifted somewhat from this figure, because of temperature effects and evaporation. Since this drift was slow and relatively uniform, it was felt that it would cause less uncertainty in the solution sensitivity than would the fluctuations involved in a continual adjustment of concentration. The concentration was measured regularly and the counting data corrected for the observed change.

The concentration of manganese sulfate was routinely monitored using the density-temperature-concentration relationship illustrated in Fig. 7. The data represented in this figure were collected through use of the following procedure: A 500 ml. volumetric flask containing a measured weight of dissolved $MnSO_4$ was diluted to the mark at a temperature of $40^{\circ}C$. The total weight of the solution was measured and the density calculated assuming the volume to be 500 ml. The flask and

contents were then progressively cooled to temperatures of 30°C, 25°C and 20°C. At each of these temperatures the volume was adjusted to the mark by adding water and the density was determined as before. This procedure was followed for concentrations of 225, 218 and 215 grams per liter to produce the data represented in the figure. Since the physical dimensions of the flask change slightly with temperature, affecting the volume of the flask, the densities are only relative except at 20°C, the temperature at which the flask was calibrated. No error is introduced into the measurements by this factor, however, because the same flask used in obtaining the calibration curves was used in the concentration measurements.

In the routine concentration checks during the course of the experiment, a density sample was drawn immediately after the counting sample. The temperature of the solution was recorded at that time. The standard 500 ml. flask was filled and adjusted to the mark with the solution from the density sample at the sampling temperature. The contents of the flask were weighed and the density calculated. With the density and temperature known, the concentration of $MnSO_4$ could be read from the graph. It was usually necessary to interpolate to temperatures other than those plotted. This interpolation could be avoided by first adjusting the flask and solution to volume at the sampling temperature and then cooling them to a lower temperature corresponding to one of the plotted curves. After adjusting the volume to the mark with water, the density of the solution was determined from its weight and the concentration read from the graph. When large interpolations were required, the density measurement was checked by this second method. Agreement in all cases was excellent.

C. Counting Technique

In order to achieve a Mn-56 counting rate sufficient to yield statistical accuracy in the neighborhood of 0.1%, it was necessary to count a large solution sample with good efficiency. A five-gallon sample size was chosen. A stainless steel container was made with a reentrant thimble in the bottom to admit a 3 in. x 3 in. NaI(Tl) scintillation counter to the center of the sample. Two separate counting channels were employed, allowing simultaneous counting of monitor foil and solution, plus interchange of samples. Each counter was mounted in a steel framework, which provided support for the heavy solution tank. A pair of steel posts at opposite corners of the framework slipped through guides mounted on the solution tank and allowed the tank to be positioned accurately without contacting the scintillator. The same guide system was used to position the monitor foil, with a pair of aluminum sleeves slipped over the posts to set the height of the foil holder. The counting arrangement is shown in Figure 8, with the solution sample on one counter and the monitor foil on the other. During the experiment the counters were enclosed in separate lead shields 4 in. thick.

The Mn-56 gamma spectrum resulting from this configuration is shown in Fig. 9, along with the spectrum observed from the monitor foil. It is immediately evident from a comparison of these two spectra that the solution and tank degrade the spectrum considerably, and shift the relative positions of the 0.85 MeV gamma ray and the valley below it. The procedure of biasing in the valley before the peak in this case leads to a considerable loss in counting rate on the one hand, and an uncertain stability due to the relative shift in valley position on the

other. For these reasons it was deemed advisable to bias at a low level so as to count the entire gamma spectrum above the noise level of the phototube. A low-noise transistorized amplifier that had been developed at Chalk River[6] for use with proportional counters was used for this purpose. To determine operating conditions for the present application, voltage plateau curves were taken for both counters on both background and Cs-137 sources. The Cs-137 source was used because its 32-keV Ba X-ray gives a convenient low energy reference point, while the background curve shows the onset of the tube noise more clearly. The Ba X-ray shows up as a step in the voltage plateau curve. The operating point chosen was on the plateau midway between the X-ray step and the onset of the tube noise as determined from the background curve. Figure 10 shows a typical set of voltage plateau curves and the associated operating point. Also shown is the plateau curve obtained using a Mn-56 source. The plateau here is much broader than those obtained with background and Cs sources, showing that the operating conditions were less stringent than the setup conditions.

The gamma counting done in this experiment was all relative, and knowledge of the absolute efficiency of the counters was not necessary for the interpretation of the data. Nevertheless it was felt worth while to know something of the counter efficiency, so a calibration program was undertaken. A vial of $MnSO_4$ powder was irradiated in the MTR and then dissolved into solution. From this solution a 1.0 ml. aliquot whose activity was approximately 10^5 dps was taken, mixed into the dead solution in the sample tank, and counted on both counters. The disintegration rate in a 0.1 ml. aliquot of the same solution was determined by both beta-gamma coincidence counting and gamma scintillation spectrometry.

The data from five trials of this experiment showed that the efficiency of Counter No. 1 was 5.24% ± .01, while that of Counter No. 2 was 5.31% ± 0.01. Since the sample tank contained approximately 2% of the solution irradiated, the overall counting efficiency for the experiment is approximately 10^{-3} counts per Mn-56 disintegration in the 250-gallon bath.

D. Experimental Procedure

Normally, irradiations were made overnight and the counting done the following day. Exceptions to this order occurred during two periods of approximately two weeks each, during which the irradiating and the counting were done in alternate 8-hour shifts. The latter arrangement allowed more rapid accumulation of data, at the expense of making the corrections for residual activity in the solution and monitor foil somewhat greater.

A day's data collection was begun with four 30-min. background counts. These yielded for each counter two counts on the decayed solution from the previous run and two background counts using the empty holder for the monitor foil. It was necessary to subtract from the counts on the old solution the contribution of the residual activity from the preceding day's irradiation. The residual activity was calculated from the previous run's observed activity, using the appropriate decay time.

The completion of the set of background counts released the sample tank for the collection of the new solution sample. The neutron beam was cut off and the mixer run for 15 minutes. Upon completion of the mixing period, the sample tank was first rinsed and then filled with the active solution. The filling was done volumetrically, the solution level being allowed to rise until the meniscus around the neck of the

tank just closed. This volumetric filling was simpler and quicker than weighing, with no loss in accuracy. After the counting sample had been drawn, an additional sample was taken for the density measurement. The solution temperature was measured at this time.

The solution sample and monitor foil were next taken to the counting area, where the first data count for the day began forty minutes after the time the beam was cut off. A total of six thirty-minute counts characterized the data, with three counts for each sample on each counter. Samples were interchanged between counters following the first, third and fifth counts. A five minute period proved adequate for reading out the data and changing samples between counts.

Following the completion of the counting schedule, the monitor foil was returned to the crystal spectrometer for inclusion in the next irradiation. Any changes in the experimental setup called for by the irradiation schedule were made at this time. If the changes required the snout to be opened, a two-minute flow of helium was used to flush the snout before the final filling to 7 lbs. gauge pressure. The irradiation tank was then filled to a standard mark in the top port and the next exposure begun.

III. Corrections to the Data

The value of eta is given closely by the ratio of solution activities observed with and without the fissionable sample in the snout. Quantitative accounting must be made for several small systematic effects before the true value of η is revealed. These corrections, ranging in size from less than 0.1% to slightly over 3%, are considered in the following paragraphs. Their calculated values are summarized in Table II.

The corrections were applied through a least squares adjustment procedure, described in Section IV below. The least squares program performed some minor adjustments in some of the corrections. The adjusted values are also shown in Table II. As might be expected, no appreciable adjustment accrued to a calculated value unless the correction involved varied during the experiment.

A. Fast Multiplication

The fissionable samples used in this experiment were desired to be approximately 0.100 in. thick so they would absorb essentially all of the thermal neutrons. Samples of this thickness will also absorb a certain number of the fission neutrons, and it proved necessary to make a correction for the fast neutron multiplication arising from the fast fission events. The magnitude of the multiplication was reduced by separating the samples into two or three foils with spaces between to increase the chance for escape of the fission neutrons. Still, the fast effect increased the number of fission neutrons absorbed in the solution by about 1.5% to 3%, depending upon the sample used.

The magnitude of the fast effect was computed for each foil by a Monte Carlo technique. The tallies from which the fast neutron multiplication was computed were those listing neutrons born of thermal fissions, neutrons escaping immediately after fission, and fission neutrons escaping following subsequent collisions in the sample. The fast effect is simply the ratio of the number of neutrons escaping from the sample to the number of neutrons originating from thermal fission. With the fast multiplication ratios known for each foil of an experimental sample, the overall fast effect can be written

$$\epsilon = \sum_i W_i \epsilon_i + \sum_{\substack{i,j \\ i \neq j}} W_i \epsilon_i P_{ij} [\epsilon_j (\frac{\eta\sigma_a + \sigma_s}{\sigma_{tr}}) - 1] \qquad (1)$$

where ϵ_i = the fast effect for the i-th foil.

W_i = the fraction of the thermal neutrons absorbed in the i-th foil.

P_{ij} = the probability that a fission neutron emerging from foil i will be absorbed in foil j.

$\eta, \sigma_a, \sigma_s, \sigma_{tr}$ = the average values of η, absorption cross section, scattering cross section, and transport cross section for fission neutrons in the sample used.

The probability P_{ij} was approximated from the formula

$$P_{ij} = \frac{N\sigma_{tr} t_j}{4} \ln(\frac{R^2 + H_{ij}^2}{H_{ij}^2}) \qquad (2)$$

where $N\sigma_{tr} t_j$ is the thickness of foil j in mean fission neutron mean free paths, R is the radius of the foil, and H_{ij} is the distance between foil centers. The corresponding interaction probability for the rectangular samples was obtained by numerical integration.

Since most of the samples used were the ones used for the Macklin-deSaussure manganese bath experiment, and the geometries were similar, it was deemed worthwhile to compute the fast effect also by their method. This method is an application of the Weinberg-Wigner formula[7] for the fast effect. The expression used is:

$$\epsilon = 1 + \frac{(\nu - 1 - \alpha) P_c \frac{\sigma_f}{\sigma_{tr}}}{1 - (\nu\sigma_f + \sigma_s)\frac{P_c}{\sigma_{tr}}} \qquad (3)$$

where ν is the number of neutrons per fission, α is the ratio of capture

to fission cross section, and σ_f, σ_s, and σ_{tr} are the fission, scattering, and transport cross sections, respectively. P_c is the probability that a fission neutron born in the sample will undergo a collision in the sample before escaping. In the present application it is assumed that this probability is the same for the first neutrons produced from thermal fission and for the neutrons proceeding from subsequent fast collisions. The interaction between samples has to be considered here too, and the value of P_c to be used is the weighted sum of the contributions of each foil:

$$P_c = \sum_{i,j} W_i [P_i + P_{ij}] \qquad (4)$$

where P_c is the total collision probability for the sample, P_i is the probability that a neutron in foil i will have a collision before it escapes from the foil, and W_i and P_{ij} are as defined previously. The individual foil collision probability, P_i, was computed in the same Monte Carlo calculation which yielded the previously discussed value of the fast effect. The values of P_{ij} were computed from Equation (2) above. The two methods agreed everywhere to better than 0.1%, with the second method yielding the higher values. The average of the two values was used in correcting the data.

The errors associated with the calculated values of the fast multiplication factor are of three sources: the uncertainty of cross sections put into the Monte Carlo program, the statistical fluctuations of the Monte Carlo process, and the uncertainty in the interaction calculations, due both to approximations involved in Equation (2) and to possible errors in the measurement of the spacing of the foils. An estimate of the error associated with cross section uncertainty was obtained by

calculating the fast effect for a U-235 foil assuming cross sections from different compilations[8-10]. Statistical analysis of the Monte Carlo results produced an estimate of the error associated with the calculation. The results of these calculations are summarized in Table III. The calculations of interaction probability were investigated by changing the spacing of the samples during the course of the experiment.

Table III

Fast Effect Calculations for U-235 Foil
Using Different Cross Section Compilations

Compilation	Fast Effect
Yiftah et al[8]	1.0133
Los Alamos[9]	1.0128
KFK[10] (Using total cross sect.)	1.0148
KFK[10] (Using transport cross section)	1.0141
Average Value	1.0138
Standard Deviation	.0009

B. Structural Absorption

There is an unavoidable loss of neutrons to absorption in the materials of which the snout and sample holders are constructed. This loss is greater for the thermal neutrons than for the fission neutrons, since the latter penetrate the solution farther on the average before undergoing absorption. To reduce the loss of thermal neutrons, an extension of the snout past the sample sphere was incorporated. This removed the impact area of the thermal beam from the vicinity of the greatest mass of aluminum. For the purpose of evaluating the structural

effects, a sheath of aluminum was added to the snout and sample holders. This added aluminum duplicated the original structure as closely as possible in mass and distribution, so the effect of the additional aluminum was equal to that of the original structure. This procedure, applied to both the thick and the thin snouts, gave two separate extrapolations to zero snout thickness. Since the U-233 and MTR Pu-239 samples used different sample holders, individual runs using extra aluminum were made with both these samples in the thick snout. Only the U-233 sample was used in the structural absorption runs with the thin snout, because all samples used in this snout used the same holder. The values and standard deviations for the various structural absorption terms, as given by the least squares program output, are summarized in Table II.

C. Indirect Multiplication

The hydrogenous bath around the sample, in addition to absorbing the fission neutrons, also acts as a reflector. Neutrons may be scattered back into the sample, where they may multiply through additional fissions. It was to minimize this effect by holding the solution away from the sample that the 6 in. diameter sphere was placed around the sample. To reduce the effect further, the samples were wrapped in cadmium except for one face, which had to be left open to admit the neutron beam. The problem then became to evaluate the effects of the cadmium. A series of irradiations were performed in which the thickness and area of the cadmium cover were altered without changing either the mass or the open area of the sample. From these data it appeared that both the area and the thickness of the cadmium had an effect on the solution activity obtained.

Accordingly, it seemed appropriate to use a correction factor employing a mass term and an area term. This factor was expressed as follows:

$$I = 1 - FM - \phi[(1-\eta)A_s + A_{Cd}] = 1 - FM - \phi A \qquad (5)$$

In this expression, M is the mass of cadmium in the wrap, A_{Cd} is the area of cadmium exposed to the reflected flux, A_s is the exposed area of the sample, and F and ϕ are the constants to be deduced from analysis of the experimental data. The factor $(1-\eta)$ takes into account the fact that a neutron striking the sample face will likely be absorbed, losing one neutron and producing η others. A is the combined area coefficient. The values determined in this manner are shown in Table I.

D. Resonance Absorption in Mn

In the thermal energy region all the competing absorbers in the manganese bath are 1/v absorbers. Under this condition the detection efficiency, in terms of Mn-56 activity per neutron absorbed, is constant with energy. In the vicinity of the manganese resonances, however, the fraction of neutrons absorbed in manganese rises. Since the fission neutrons must pass through this resonance energy region in slowing down, they produce relatively more Mn-56 activity per absorption than do the thermal neutrons.

Since it is only the above-1/v portion of the resonance integral that contributes to the change in absorption fraction, the correction was expressed in terms of the thermal absorption cross sections and the above-1/v components of the resonance integrals. The factor by which the solution activity is raised by resonance absorption may be written as

$$R = 1 + \frac{1}{\overline{\Sigma_s \xi}} \left[\frac{I_a^{Mn}}{\Sigma_a^{Mn}} (\Sigma_a^H + \Sigma_a^S) - I_a^S \right] \qquad (6)$$

where $I_a^{Mn} + I_a^S$ are the above-1/v components of the macroscopic resonance integrals of Mn and S, respectively. Σ_a^{Mn}, Σ_a^H, and Σ_a^S are the macroscopic absorption cross sections of Mn, H, and S and $\Sigma_s \xi$ is the composite product of scattering cross section times logarithmic energy decrement for the solution.

While there is a fairly wide spread in the reported values[11-14] for the above-1/v resonance integral of manganese, the recent values[13-14], for which the highest accuracy is claimed, appear to agree that a good estimate of the integral is 8.0 ± 0.5 barns. The fraction I_a^{Mn}/Σ_a^{Mn} is then $0.60 \pm .06$. For the solution used in this experiment the values of the remaining parameters are: $\overline{\Sigma_s \xi} = 1.323$, $\Sigma_a^H = 0.0217$, $\Sigma_a^S = 0.00045$, and $I_a^S = 0.00033$. An error of about 1% is estimated for these latter quantities. The correction for the effect of resonance absorption in manganese then takes the value 1.0098 ± 0.0020.

E. Transmission

Although the samples were almost totally absorbing, the transmissions were not quite zero for any of them. The transmitted neutrons were absorbed in the cadmium backing, and so contributed to neither Mn activation in the solution nor fission in the sample. The transmissions of the foils used were individually measured on the crystal spectrometer in the same neutron beam and at the same energies used in the η experiment. Those samples having integrally mounted cadmium backing could not be measured at these energies, but their thicknesses were compared to those of the unbacked samples by means of transmission measurements above the Cd cutoff. This

comparison could be only approximate, since it was not possible to make a precision measurement of the transmission of the Cd backing enclosed in the sample.

The transmission measurements disclosed a degree of non-uniformity in foil thickness. The U-235 foils appear to be uniform within .001 in. or less, but the U-233 foil measurements indicated a spread of .002 in. in thickness and the Pa-239 foils indicated a .003 in. spread. While the nominal thicknesses of all foils were 0.025 in., the averages appear to be .023 in. for the U-235 foils, .027 in., for the U-233 foils, and .020 in. for the round Pu foils. The rectangular Pu sample consisted of two foils .015 in. and .070 in. thick.

The transmission corrections and their errors, as indicated by the measurements, are shown in Table IV. The corresponding correction used in the least squares analysis was the product of the transmission and sample purity corrections. Neither the experiment nor the analysis was designed to differentiate between the two effects.

Table IV

Transmission Correction

Isotope	0.025 eV	.057 eV
U-233	.9994 ± .0001	.9931 ± .0001
U-233 (2-foil sample)		.9155 ± .0001
U-235	.9996 ± .0001	
Pu-239 (both samples)	1.0000 ± .0001	.9998 ± .0001

F. Scattering

A second cause of the failure of the samples to be totally absorbing is that some neutrons are scattered out of the sample. If a fraction s/N

of incident neutrons are scattered from the sample, and a fraction W of these are absorbed in the solution, the effect on a material of value η is

$$S = 1 - \frac{s}{N}\left(\frac{\eta - W}{\eta}\right) . \qquad (7)$$

It was assumed that only the neutrons scattered out of the incident face of the sample would be asorbed in the solution. Those scattered out the back are absorbed in the Cd wrapping.

The fractions of neutrons scattered out of the front and back of the samples were computed using the analytical expressions in terms of exponential integrals[15]. The Monte Carlo calculation also yielded the probability of escape of the scattered neutrons. These results agreed with those from the analytical calculation, within the limits of statistical error of the Monte Carlo calculation.

The scattering corrections applied in the experiment are summarized in Table II. The errors quoted are estimated from the uncertainties in cross sections and in the fraction W.

G. Duct Streaming

The channel through which the neutron beam entered the sample chamber also formed a path for neutrons to escape from the tank. Since this loss was small, it was approximated by the solid angle subtended at the sample by the mouth of the neutron channel.

H. Leakage

The manganese bath is not truly infinitely thick, and some neutrons can escape through the solution. Leakage calculations were made by Dr. Herbert Goldstein[16], using several techniques including Monte Carlo, moments method, and a computer-programmed solution to the Boltzman equation.

The geometry used in these calculations took into consideration the void around the sample, assuming spherical symmetry throughout. Since the real tank is cylindrical, some approximations had to be made to adapt the Goldstein calculations to the physical situation. The leakage was taken to be the value shown by the calculations for a thickness of solution equal to the average thickness of the cylindrical solution. The value obtained in this manner is 0.9988.

In addition to the spherical approximation, use of the Goldstein calculations directly involved another uncertainty. The calculations assumed that the solution continued infinitely beyond the point for which the leakage figure was given, and the neutrons were followed in energy down only to 1 eV. The error introduced in the leakage value by these factors should be small, since the leakage itself is small and the borated paraffin shield around the tank approximates the solution as a reflector for the above-1 eV neutrons considered in the calculations. Nevertheless, the quoted error for this leakage correction is arbitrarily increased from the 11% error associated with the calculation alone to 100% of the leakage itself, making the leakage correction 0.9988 ± 0.0012.

I. High Energy Absorption

Partially compensating the excess resonance absorption in Mn is the loss of neutrons to high energy reactions in the oxygen and sulfur in the Mn bath. The calculations by Goldstein for the leakage factor[16] also yielded the fractional loss of neutrons to these high energy reactions. These calculations showed a loss to O(n,p) and O(n,α) reactions of 0.48%, and to S(n,p) 0.11% of the source neutrons. The correction for high energy absorption is thus 0.9941 ± 0.0005.

J. Impurities

The measured value of η is affected by any impurities in the sample which absorb neutrons but do not produce the same number of fission neutrons as the principal isotope of the sample. The correction for this effect is straightforward, consisting simply of the ratio of the number of neutrons actually produced in the sample to the number that would be produced if all components of the sample had the same value of η as does the principal isotope. The analytical expression is

$$I = \frac{\Sigma N_i \sigma_i \eta_i}{\eta \Sigma N_i \sigma_i} \tag{8}$$

where N_i, σ_i, and η_i are the number of nuclei per cubic centimeter, the absorption cross section, and the value of η for the i-th component of the sample. The principal isotope of the sample is specified by $i = 0$.

Since the samples used in this experiment were all prepared at other laboratories, no independent determination of the sample composition was made at the National Reactor Testing Station. The sample compositions, as supplied by the laboratories of origin of the samples, are given in Table V. Also shown in Table V are the correction factors for impurities associated with each sample.

IV. Interpretation of Data

The key numeric extracted from the data for each irradiation was the ratio of solution activity to monitor activity. This ratio was computed separately for each counter, since small differences in size and mounting of the two crystals gave them slightly different efficiencies for the two types of samples counted. Each count was

corrected for counting background and for decay since the termination of the irradiation. Counts of the same type, characterized by the counter and sample involved, were weighted by the inverse of their statistical variances and averaged. Each average was corrected for residual activity, as calculated from the activity observed for the previous irradiation and the decay time since that observation. From the corrected average, the ratio of solution activity to monitor foil activity was calculated for each counter's data.

Irradiation backgrounds were measured by irradiating the solution with a cadmium filter between the monitor foil and the tank. This position for the cadmium filter was chosen because it allowed easier insertion and removal of the filter than did a position inside the sample sphere, and the two positions yielded the same background determination. In fact, a criterion for alignment of the system was that the background obtained with the filter outside should be indistinguishable from that using a sample-sized cadmium filter at the sample position. A 0.020 in-thick cadmium filter allowed about 0.5% of the beam to pass through, but with a 0.040 in-thick filter there was no observable difference in irradiation background between the U-233, U-235, and open beam irradiations. On the other hand, the backgrounds for the Pu-239 samples were slightly higher because of the spontaneous fission activity of the Pu-240 contaminant in these samples. In both cases the irradiation backgrounds were about 5% of the foregrounds. The irradiation backgrounds were subtracted from the solution-to-monitor ratios of the data runs.

The use of the manganese monitor removed from the solution-to-monitor ratios any dependence upon neutron beam strength. The measured numerics depended upon η and the quantities tabulated in the list of corrections, in combinations depending upon the particular setup of the individual irradiations.

The least squares method described by Cohen, Crowe, and DuMond[17] is ideally suited to the task of analyzing the data from a many-parameter experiment such as the present one. To apply this method, the result of each irradiation was expressed as an equation in which the product of the factors affecting the solution-to-monitor ratio was equated to that ratio. The equations were then linearized. As an example of the procedure followed, consider the type of equation describing the irradiations made with the U-233 sample, using aluminum spacers and 0.005 in. cadmium wrap, in the heavy snout at 0.025 eV neutron energy:

$$R = K\eta S \epsilon (1 - MF - \emptyset A)XDTQ \qquad (9)$$

Here R is the solution-to-monitor ratio, K is a factor describing the relative efficiency of the counter for the solution and monitor samples, and η is the value of η for U-233. The other factors are corrections for scattering, fast effect, indirect multiplication, structural absorption, duct streaming, a sample-dependent factor involving transmission and purity considerations, and a solution-dependent factor including resonance absorption in manganese, high energy parasitic absorption, and leakage. The equation is linearized by making variable changes of the form $K = K_o(k + 1)$. In this substitution, k is the linearized variable and K_o is a constant, called the origin value of variable K. R_o is

defined as the value of R that will satisfy the equation when origin values are used throughout the right hand side of the equation.

When the substitutions are made in the equation, a linearized equation results, provided that the origin values have been chosen in such a manner as to make the linearized variables small enough that products of two or more of these variables can be neglected. The linearized equation represents a hyperplane approximating in the vicinity of the origin the true surface represented by Equation (9). Ideally, the planes of all the equations of the experiment should intersect at the same point. Because of errors associated with the experiment, the planes do not actually intersect in such a point, but form an envelope of a small region. The least squares technique locates the point within that region that is most likely to be the point of intersection if all error could be removed from all parts of the experiment.

In order for the least squares method to give best values and variances for the variables, it is necessary to have more equations than variables; i.e., that the system be overdetermined. To solve the overdetermined system, the set of equations must be reduced to a set of normal equations, equal in number to the number of variables. Each equation is multiplied by a weighting factor proportional to the reciprocal of the variance associated with its numeric, and by the coefficient of the first variable. The resulting equations are added to produce one of the normal set. The other normal equations are obtained similarly, but using as multipliers the coefficients of the remaining variables in order. The solution of the set of normal equations gives the best estimate of the values of all the variables. Inversion of the matrix of

the normal equations yields the covariance matrix whose elements are the variances and covariences associated with the solution of the direct matrix.

The array of data for the measurements at 0.025 eV comprised 39 variables in 154 equations. Of these equations, 130 described the results of irradiations and 24 specified the values and variances calculated for corrections. The corresponding system at 0.057 eV contained 26 variables in 103 equations, 86 being experimental equations and 17 auxiliary calculated data.

An IBM 7040 computer was used to perform the least squares analysis. In addition to solving the system of equations, the computer was programmed to compute the value of chi-square for the system. Chi-square is given by

$$\chi^2 = \Sigma\left[\frac{C_u - C_u^*}{\sigma_u}\right]^2 \qquad (10)$$

where C_u and C_u^* are the input and output values of the numerics of the equations. A measure of how well the data fit the assumed statistical distribution is given by the value of chi-square, which should be equal to the number of degrees of freedom of the system. The number of degrees of freedom is given by the difference between the number of equations and the number of unknowns in the system. The ratio of chi-square to the number of degrees of freedom is expected to be unity. For the data at 0.057 eV this ratio was 1.7 which, though a bit high, is still statistical at the 0.05 level. On the other hand the data at 0.025 eV showed a ratio of 3.5 between chi-square and the degrees of freedom. This ratio is highly unlikely statistically, and indicates either an underestimate of error or the existence of systematic errors in the experiment. Some equipment problems were indeed encountered during the course of this phase of the

experiment, and a few data were discarded when a malfunction could be pinpointed with certainty. The sample sizes were in general too small for the application of outrider tests to indicate erroneous values in the remaining data. Therefore all these data were retained, with the variances being multiplied by the indicated factor 3.5. The rerun of the least-squares analysis showed the values changed very little, but the ratio of chi-square to number of degrees of freedom dropped to a comfortable 1.08.

Since the correction factors to the experiment were treated as variables in the least squares analysis, these factors underwent some adjustment from their calculated values. Table II summarized the calculated values of the corrections and the least-squares adjusted values, along with the estimated standard deviations in each case.

V. Conclusions

The values and standard errors for η for the three isotopes are summarized in Table VI. The errors shown here, and throughout this report, represent one standard deviation in the quantity at hand. Also given in Table VI are ratios between the values of η for the various isotopes. Table VII shows a comparison between these results and those of the Oak Ridge manganese bath experiment[2], along with the values given by the recent least squares analysis by Sher and Felberbaum[18]. This analysis did not include the present results. The drop in η for Pu-239 from 0.025 to 0.057 eV is in good agreement with the energy variation curve fit by Leonard[19] to the existing data. The apparent change in η for U-233 from 0.025 eV to 0.057 eV is within the standard deviations of the quantities involved. Nevertheless, the commonality of the measurements suggest that there is a true decrease in η as the neutron energy increases in this region.

VI. Acknowledgments

The authors would like to acknowledge the very valuable assistance of many people through the many phases of this experiment. In particular, they would like to thank Mr. R. A. Gideon for programming and running the least squares analysis of the data, Mr. C. L. Miller for construction and care of electronic equipment besides assisting in the collection of data, Messers D. McConnell, D. I. Hagen, R. D. Vesser, and E. H. Magleby for assisting in the data collection, and Dr. R. S. Shankland for valuable discussions.

VII. References

1. CINDA, An Index to the Literature on Microscopic Neutron Data, EANDC 46 "U" (1965).

2. R. L. Macklin, et al, "Manganese Bath Measurements of Eta of U-233 and U-235," Nucl. Sci. Eng. 8, 210 (1960).

3. J. R. Smith and H. G. Miller, A Mechanical Neutron Filter for a Crystal Spectrometer, IDO-16878 (1963).

4. H. J. Hay, The Importance of Multiple Bragg Scattering for Neutron Crystal Spectrometers, AERE-R 2982 (1959).

5. J. G. Dash and H. S. Sommers, Jr., "A High Transmission Slow Neutron Velocity Selector," Rev. Sci. Instr. 24, 91 (1953).

6. J. B. S. Waugh, A Transistor Amplifier for use with Methane Proportional Counters, CREL-828 (1959).

7. A. M. Weinberg and E. P. Wigner, The Physical Theory of Neutron Chain Reactors, Chapter XX, p. 696, University of Chicago Press, Chicago (1958).

8. S. Yiftah, et al, Fast Reactor Cross Sections, Pergamon Press (1960).

9. Los Alamos Group-Averaged Cross Sections, LAMS 2941 (1963).

10. J. J. Schmidt, Neutron Cross Sections for Fast Reactor Materials, Part II: Tables, KFK 120 (1962).

11. R. L. Macklin and H. S. Pomerance, "Resonance Capture Integrals," Prog. in Nuclear Energy, Ser. 1, Vol. 1, p. 179 (1956).

12. R. B. Tattersall, et al, Pile Oscillator Measurements of Resonance Absorption Integrals, AERE-R 2887 (1959).

13. W. H. Walker, et al, Can. J. Phys. 38, 57 (1960).

14. R. Dahlberg, et al, J. Nucl. Energy 14, 53 (1961).

15. K. M. Case, et al, "Introduction to the Theory of Neutron Diffusion," Vol. 1, p. 17, U. S. Government Printing Office, Washington, D. C. (1953).

16. H. Goldstein, "Calculations of Neutron Leakage and High Energy Absorption in a Manganese Sulfate Bath," Trans. Am. Nuclear Soc. 5, 89 (1962).

17. E. R. Cohen, et al, The Fundamental Constants of Physics, Interscience Publishers, Inc., New York (1957).

18. R. Sher and J. Felberbaum, Least Squares Analysis of the 2200 m/sec Parameters of U-233, U-235 and Pu-239, Final Report, BNL 918 (1965).

19. B. R. Leonard, Jr., "The Low Energy Cross Sections of Fissile Nuclides," in Neutron Physics, edited by M. L. Yeater, Academic Press, New York (1962).

Figure Captions

Figure 1 - Time-of-flight analyses of neutron beams used in the experiment. No higher order peaks are evident in either spectrum.

Figure 2 - Schematic view of experimental arrangement.

Figure 3 - Photograph of tank, collimator and mechanical neutron filter.

Figure 4 - The two sample snouts used in the experiment. The tube in the center is the sample holder for the light snout, shown at left.

Figure 5 - The two sample holders used with the heavy snout. The holder on the left is for use with the rectangular Pu-239 samples. The holder on the right accommodates the round samples obtained from Oak Ridge.

Figure 6 - Schematic diagram of sample configuration. For dimensions see Table I.

Figure 7 - Variation of observed density of $MnSO_4$ solution with concentration and temperature.

Figure 8 - Counter arrangement showing sample positioning devices. The five-gallon solution sample is shown on the counter at the left, while the monitor foil is positioned on the counter at right.

Figure 9 - Gamma ray spectra from Mn^{56}. Curve A shows the spectrum from the monitor foil, while Curve B shows the distorted spectrum observed from the solution sample.

Figure 10 - Voltage plateau curves obtained using 3 in. x 3 in. NaI(Tl) scintillation counter: (A) Mn^{56} spectrum from monitor foil (B) Cs^{137} and (C) Room background.

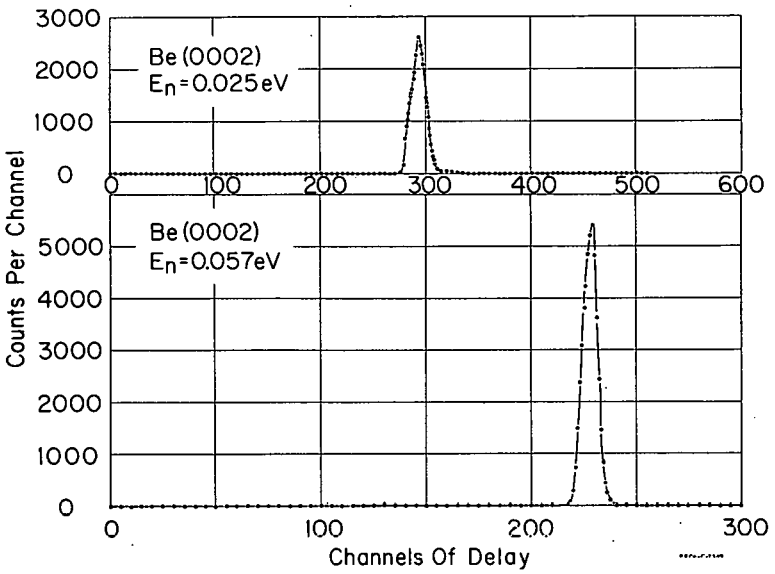

Figure 1

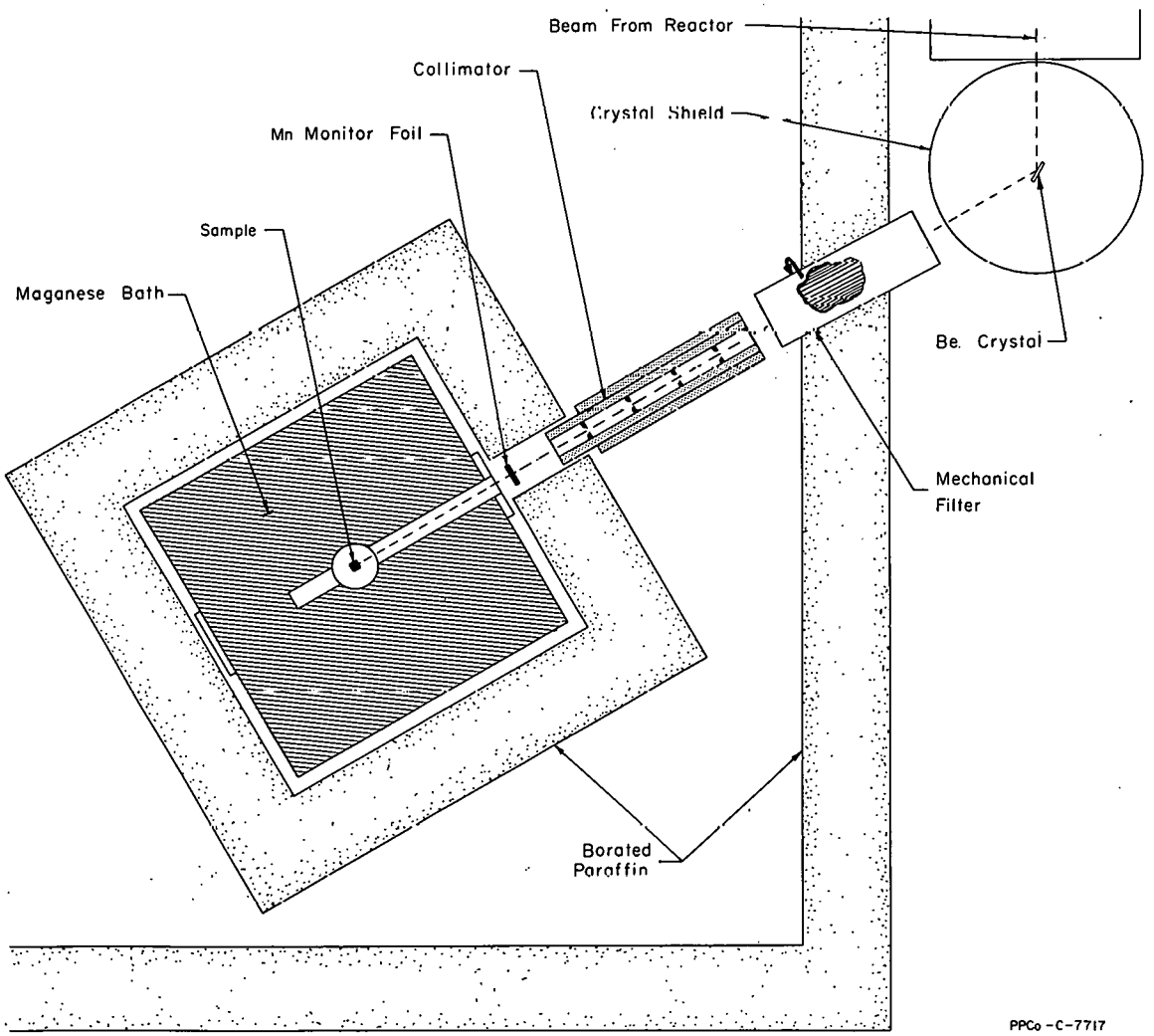

Figure 2

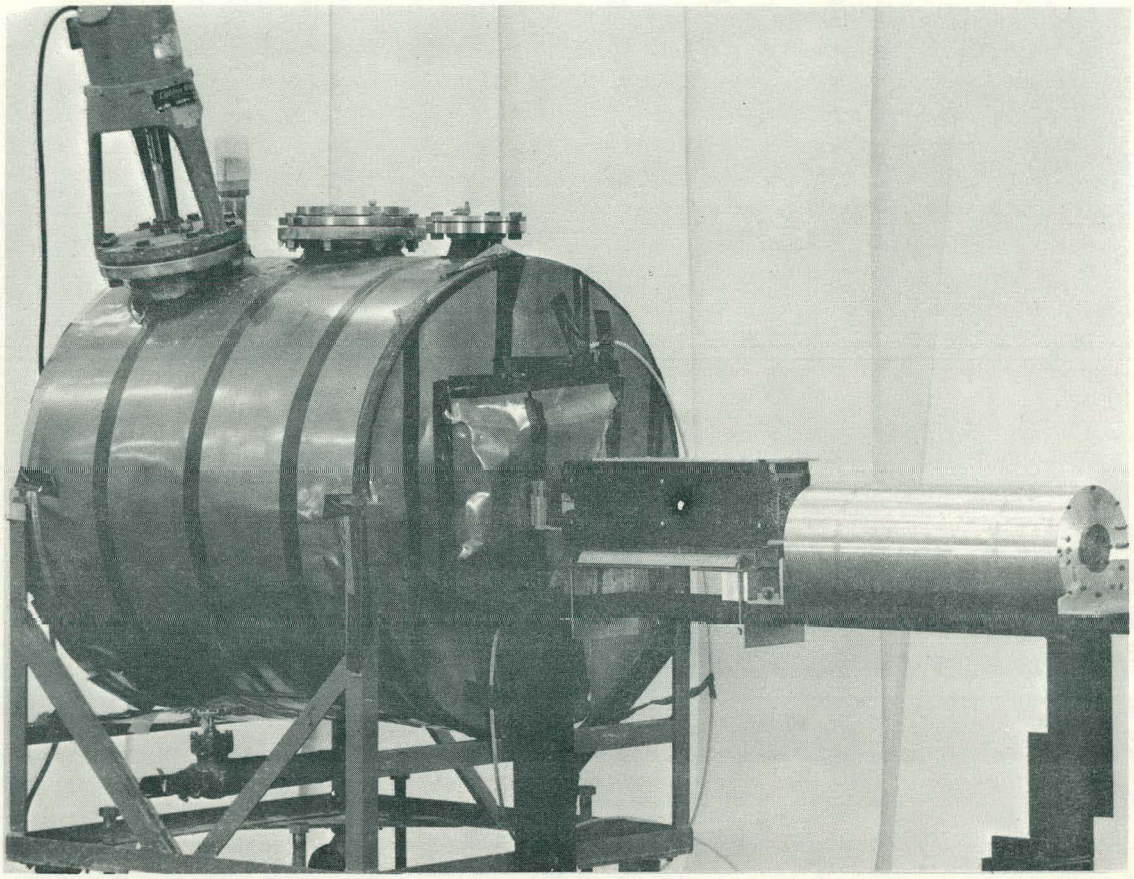

Figure 3

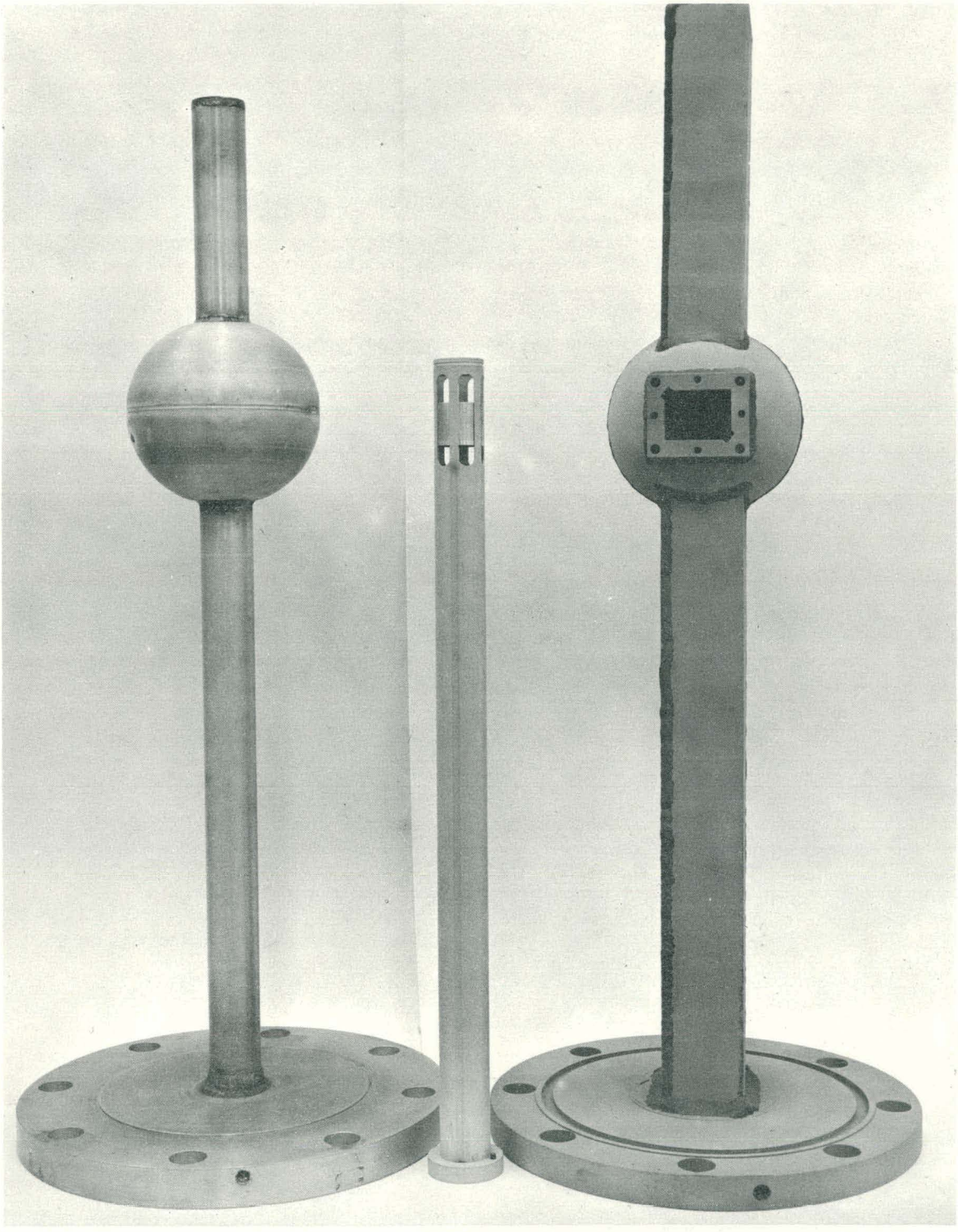

Figure 4

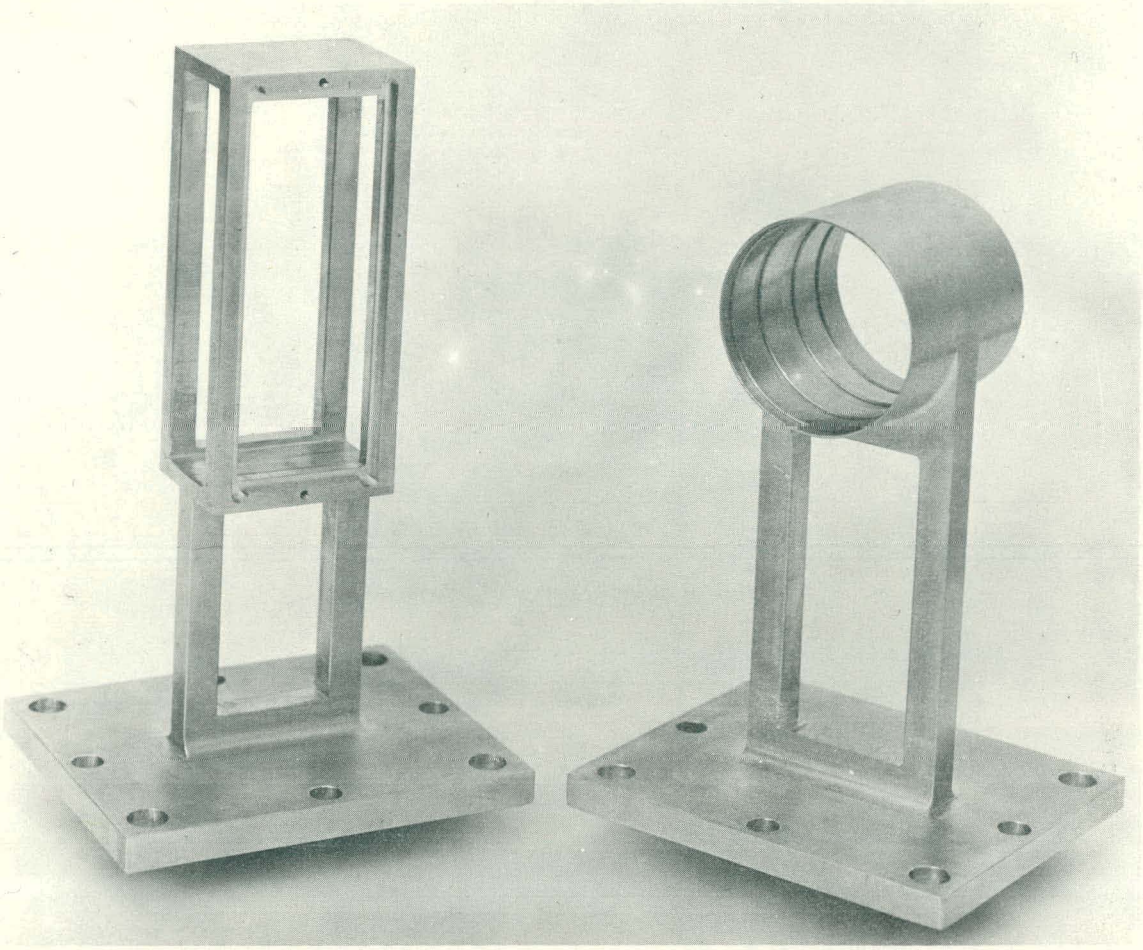

Figure 5

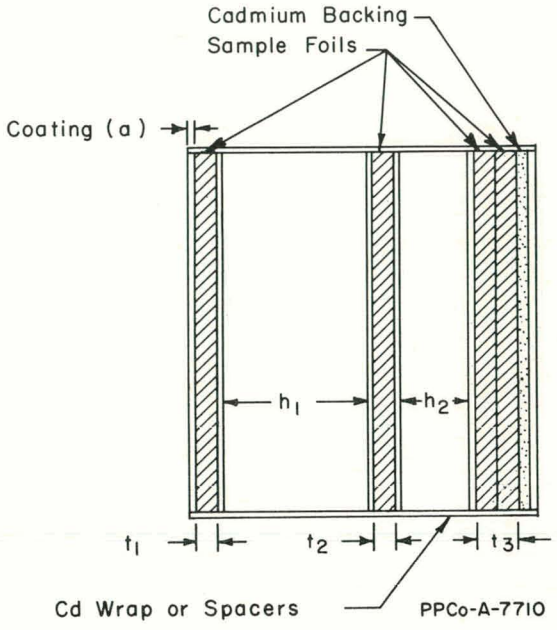

Figure 6

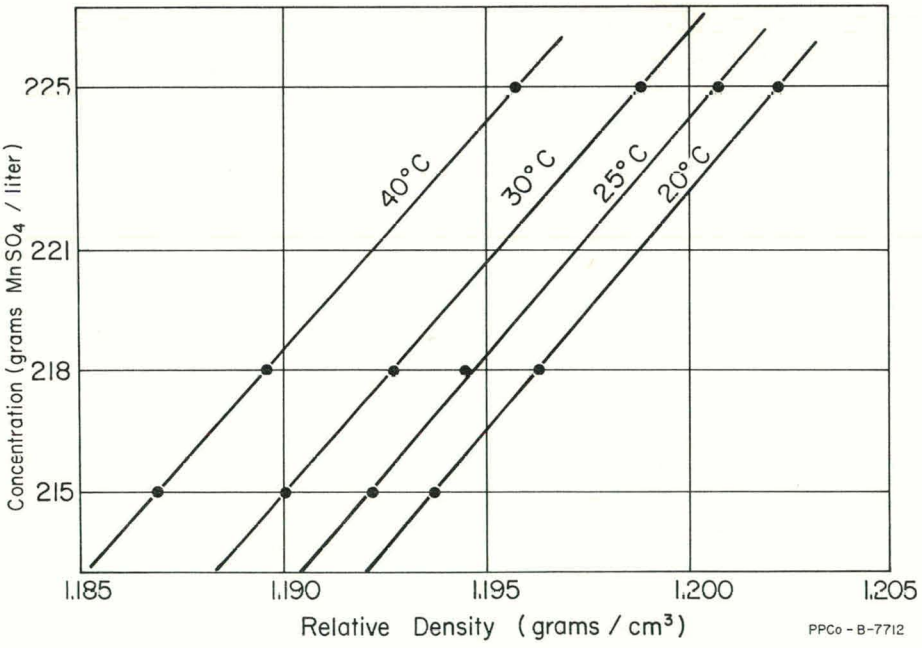

Figure 7

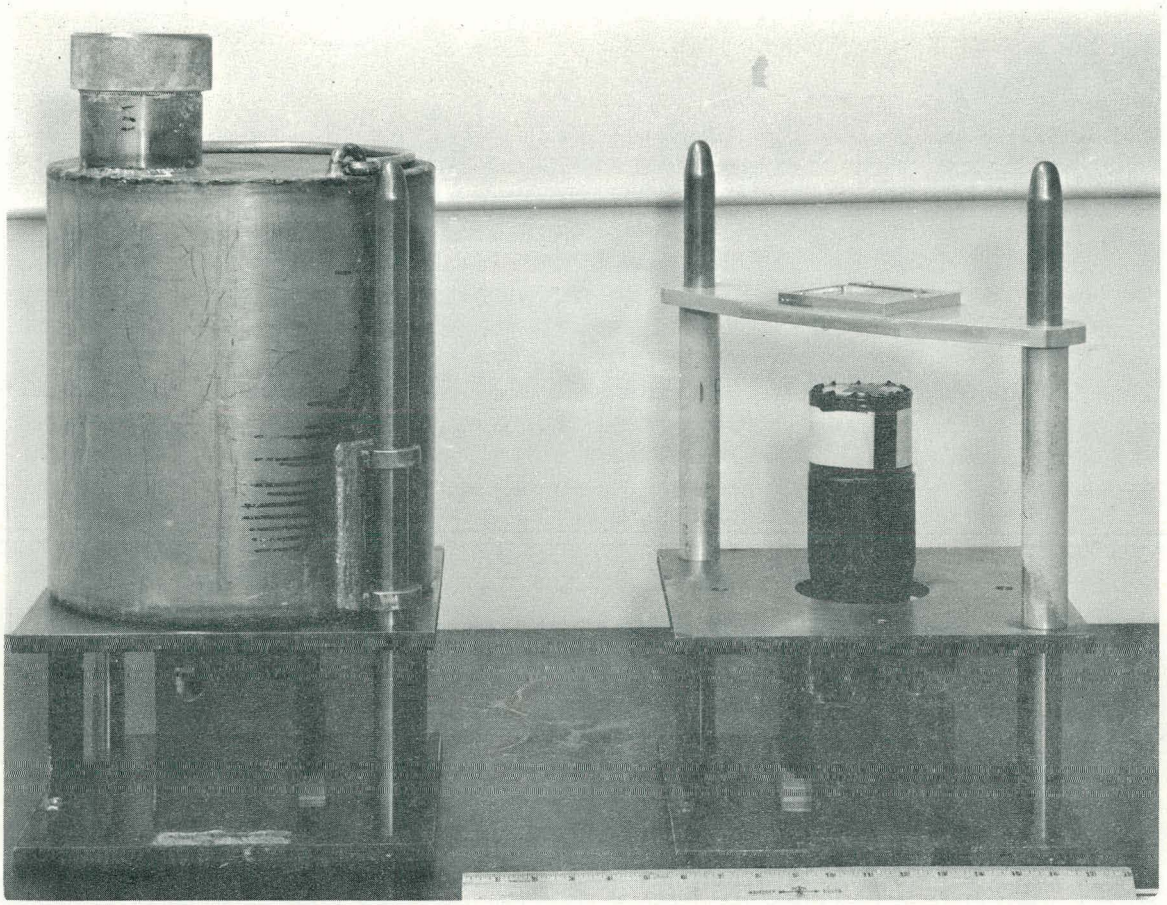

Figure 8

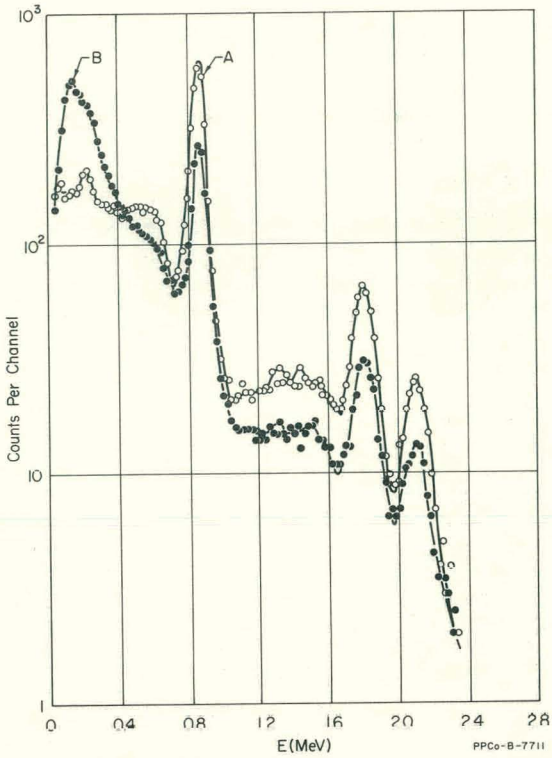

Figure 9

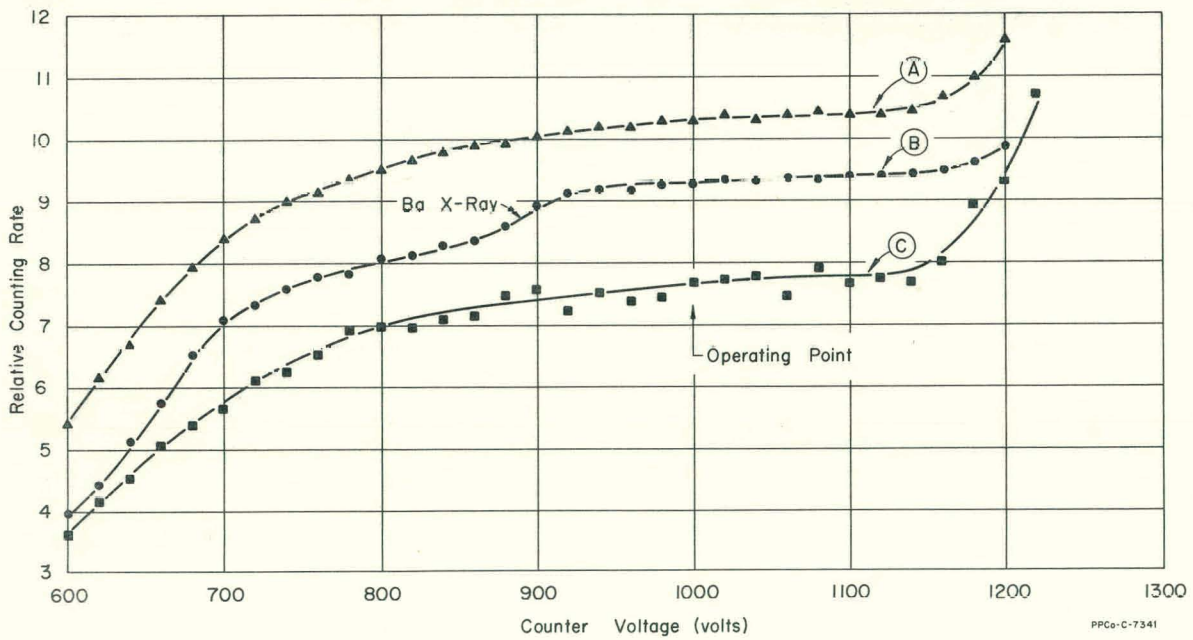

Figure 10

Table I

Sample Configurations*

Sample	Shape	Spacers	a(cm)	t_1(cm)	t_2(cm)	t_3(cm)	h_1(cm)	h_2(cm)	Cd(cm)
U-233 A	round**	Al	0.020 Al	0.066	0.068	0.132	1.48	0.85	0.051
U-233 B	round	Short Cd	.020 Al	0.066	0.068	0.132	1.61	.87	.051
U-233 C	round	Long Cd	.020 Al	0.066	.068	.132	2.72	2.10	.051
Pu-239 A	round	Al	.020 Al	.049	.047	.090	1.48	.85	.051
Pu-239 B	round	Long Cd	.020 Al	.049	.047	.090	2.72	.85	.051
Pu-239 C	rect.***		.013 Ni	.038	.170	none	2.30	none	none
U-235	round	Long Cd	.020 Al	.058	.058	.116	2.72	2.10	.051

*See Figure 6 for identification of dimensions

**Round samples are 3.65 cm diameter

***Dimensions 7.04 x 2.70 cm

Table II

Corrections to the Experiment
Calculated Values and Adjusted Values
from Least Squares Data Analysis

I. E = 0.025 eV

EFFECT	CALCULATED VALUE	ADJUSTED VALUE
A. Fast Effect*		
U-233 A	1.0307 ± 0.0020	1.0311 ± 0.0013
U-233 B	1.0299 ± .0020	1.0279 ± .0014
U-233 C	1.0266 ± .0020	1.0265 ± .0016
U-235	1.0149 ± .0020	1.0149 ± .0007
Pu-239 A	1.0293 ± .0020	1.0290 ± .0016
Pu-239 B	1.0267 ± .0020	1.0290 ± .0016
Pu-239 C	1.0237 ± .0020	1.0217 ± .0016
B. Structural Absorption#		
1. Heavy Snout		
a. Open beam, round holder		0.9690 ± .0020
b. Fission neuts., round sample		.9932 ± .0019
c. Open beam, rect. holder		.9656 ± .0018
d. Fission neutr. rect. holder		.9949 ± .0023
2. Light Snout		
a. Open beam		.9886 ± .0016
b. Fission neuts.		.9992 ± .0017
C. Scattering		
1. U-233	.9966 ± .0014	.9966 ± .0014
2. U-235	.9967 ± .0020	.9967 ± .0020
3. Pu-239 (round)	.9986 ± .0014	.9986 ± .0012
4. Pu-239 (rect.)	.9988 ± .0012	.9987 ± .0012
D. Sample Effects%		
1. U-233	.9993 ± .0010	.9993 ± .0010
2. U-235	.9994 ± .0010	.9994 ± .0010
3. Pu-239 (round)	.9943 ± .0010	.9943 ± .0010
4. Pu-239 (rect.)	.9941 ± .0010	.9940 ± .0010

*Description of samples given in Table I.

#No calculated values.

%Transmission and impurities.

Table II (cont.)

EFFECT	CALCULATED VALUE	ADJUSTED VALUE
E. Solution Effects[†]	1.0023 ± .0024	1.0023 ± .0024
F. Cd. Wrap Effects (x 10^4)		
1. F (mass coef.)	2.08 ± .25	2.11 ± .29
2. ϕ (area coef.)	2.72 ± .07	2.73 ± .12
G. Duct Streaming		
1. Heavy Snout	.9987 ± .0005	.9987 ± .0002
2. Light Snout	.9997 ± .0002	.9997 ± .0002
II. E = 0.057 eV		
A. Fast Effect[*]		
U-233 A	1.0320 ± 0.0020	1.0319 ± 0.0013
U-233 (2-foil sample)	1.0408 ± .0020	1.0409 ± .0016
U-233 (no spacers)	1.0559 ± .0020	1.0562 ± .0015
Pu-239 C	1.0326 ± .0020	1.0323 ± .0017
Pu-239 C (reversed)	1.0598 ± .0020	1.0601 ± .0017
B. Structural Absorption[#] (Heavy snout only)		
1. Open beam		0.9723 ± .0019
2. Fission neuts., U-233		.9948 ± .0010
3. Fission neuts., Pu-239		.9933 ± .0013
C. Scattering		
1. U-233 A	0.9941 ± 0.0015	0.9939 ± 0.0013
2. U-233 (no spacers)	.9969 ± .0010	.9970 ± .0009
3. U-233 (2-foil sample)	.9957 ± .0010	.9957 ± .0009
4. Pu-239 C	.9978 ± .0015	.9976 ± .0014
5. Pu-239 C (reversed)	.9989 ± .0010	.9990 ± .0010
D. Sample Effects[%]		
U-233 A	.9930 ± .0011	.9930 ± .0010
U-233 (2-foil sample)	.9154 ± .0011	.9154 ± .0010
Pu-239	.9937 ± .0014	.9937 ± .0014

[†] Leakage, Mn resonance absorption, and high energy absorption in O and S.

[*] Description of samples given in Table I.

[#] No calculated values.

[%] Transmission and impurities.

Table II (cont.)

	EFFECT	CALCULATED VALUE	ADJUSTED VALUE
E.	Solution Effects[‡]	1.0010 ± .0024	1.0010 ± .0024
F.	Cd Wrap Effects ($\times 10^4$)[#]		
	F (mass coef.)		2.08 ± .25
	ϕ (area coef.)		2.72 ± .07

[‡] Leakage, Mn resonance absorption, O and S high energy absorption, and duct streaming.

[#] No calculated values.

Table V

Composition of Samples

A. U-233 Sample

U-232	.6 ppm	
U-233	99.76 ± 0.01%	
U-234	0.022 ± .001%	Total Uranium 99.97 ± 0.2%
U-235	0.07 ± .0007%	
U-236	1 ppm	Others ≤ 0.23%

Impurity correction 0.9999 ± .0010

B. U-235 Sample

U-234	0.10 ± .02%	
U-235	99.70 ± .05%	Total Uranium 99.40 ± 0.2%
U-236	0.11 ± .11%	
U-238	0.10 ± .10%	Others <0.7%

Impurity correction 0.9998 ± .0010

C. Pu-239 Sample (round)

Pu-238	0.003%	
Pu-239	97.90	Total Pu: 98.90 ± 0.2%
Pu-240	2.01	Al: 0.95
Pu-241	0.06	Others: 0.1

Impurity correction .9943 ± .0010

D. Pu-239 Sample (rectangular)

Pu-238	0.02%	
Pu-239	97.53%	
Pu-240	2.36	Total Pu: 98.80%
Pu-241	0.10	Al: 1%
Pu-242	0.05	Others: 0.2%

Impurity correction 0.9941 ± .0010

Table VI

Summary of Results

	E = 0.025 eV		E = 0.057 eV	
Isotope	η	Ratio to U-235	η	Ratio to U-233
U-233	2.298 ± 0.009	1.105 ± 0.005	2.288 ± 0.009	
U-235	2.079 ± 0.010			
Pu-239	2.108 ± 0.008	1.014 ± 0.005	2.034 ± 0.009	0.889 ± 0.005

Table VII

Comparison of 0.025 eV Values With Other Work

	U-233 η	U-235 η	Pu-239 η	η23/η25	η49/η25
Present Experiment	2.298 ± .009	2.079 ± 0.010	2.108 ± 0.008	1.105 ± .005	1.014 ± .005
Macklin et al (Mn bath expt.)	2.296 ± .010	2.077 ± .010	2.143 $^{+\ .010}_{-\ .020}$	1.105 ± .005	1.032 $^{+\ .006}_{-\ .009}$
Sher and Felberbaum (least squares anal.)	2.292 ± .006	2.078 ± .005	2.116 ± .009	1.103 ± .003	1.0183 ± .0041

PHILLIPS
PETROLEUM
COMPANY

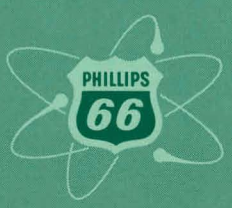

ATOMIC ENERGY DIVISION